photonics

Communication

Saturated Gain-Induced Non-Reciprocal Transmission and Broadband On-Chip Optical Isolator

Mingyuan Xue [1,2,*], Haojiang Tong [1,2], Hao Dong [3] and Meijia Wang [2]

[1] Shaanxi Joint Laboratory of Artificial Intelligence, Shaanxi University of Science and Technology, Xi'an 710021, China
[2] The School of Electronic Information and Artificial Intelligence, Shaanxi University of Science and Technology, Xi'an 710021, China
[3] The School of Physics and Information Science, Shaanxi University of Science and Technology, Xi'an 710021, China
* Correspondence: xuemy@sust.edu.cn

Abstract: To overcome the limitation of dynamic reciprocity, a new method for designing broadband on-chip optical isolators is proposed and demonstrated based on saturated gain, which is able to support simplex and duplex operation modes. By connecting a saturated gain waveguide to an appropriate linear loss waveguide, broadband isolation is predicted and proved theoretically through saturated gain-induced non-reciprocal transmission. The proposed isolator is numerically demonstrated with an operating band of 59 nm and an isolation ratio of −20 dB at the central wavelength of 1550 nm. It is noteworthy that when the current pump changes, the isolator still works well and keeps the high isolation ratio at a different input power. The footprint of the whole device is 465 μm × 0.35 μm which satisfies the requirement of photonic integrated circuits. The proposed isolator, with the combined advantages of compact footprint, broadband, duplex operation and high isolation, can enable on-chip unidirectional transmission and complex topological routing designation.

Keywords: optical isolator; reciprocal; saturated gain; on-chip; broadband

check for updates

Citation: Xue, M.; Tong, H.; Dong, H.; Wang, M. Saturated Gain-Induced Non-Reciprocal Transmission and Broadband On-Chip Optical Isolator. *Photonics* **2024**, *11*, 261. https://doi.org/10.3390/photonics11030261

Received: 1 February 2024
Revised: 25 February 2024
Accepted: 8 March 2024
Published: 14 March 2024

1. Introduction

Non-reciprocity is a remarkable physical phenomenon, which provides abundant applications in the photonics industry [1–8], especially on-chip photonics. The photonic isolator is one of the biggest concerns in non-reciprocal on-chip photonic devices due to wide applications of integrated backscatter eliminating and complex communication topology construction in photonics. To implement on-chip isolation, three well-known non-reciprocal phenomena have been investigated extensively as solutions, including nonlinear optical (NLO) effects [9–13], magneto-optical (MO) effects [14–22] and the time-dependent optical (TDO) system [23–25]. The NLO effects usually provide two schemes, which are optically induced transparency [8] and optical bistability [9,10]. The former exploits four-wave mixing in micro-ring which leads to the narrow operation band. The latter is seriously limited by dynamic reciprocity [26], and hence, the isolator function cannot be constructed when a forward signal transmits through the system, which means the duplex operation modes cannot be supported. The MO effects are also actualized by two schemes. One is an MO micro-ring [12], which is not only a narrow operation band device but also requires complex manufactured technology. The other is the MO-induced reciprocal loss waveguide [14,18], which is limited by its large size for on-chip photonics. The TDO system demands a very high modulation frequency. Therefore, although numerous pieces of research focus on optical isolators, there is still a lack of a small-sized scheme holding not only a wide operating band but also supporting duplex workings and keeping a high isolation rate.

In this paper, we propose and demonstrate that saturated gain can be a new solution to implement non-reciprocal transmission, which is a fabrication-friendly, duplex work supporting, wide operating band and relatively small-sized scheme. Table 1 shows the comparison between current schemes and the saturated gain-induced non-reciprocal transmission proposed in this paper.

Table 1. Characteristics of the current schemes and proposed scheme.

	Fabrication	Duplex Working	Operating Band	Size
NLO	Easy	No	Narrow (~1 nm)	~100 μm
MO micro-ring	Very Hard	Yes	Narrow (<1 nm)	~100 μm
Normal MO	Easy	Yes	Wide (>50 nm)	>1 mm
TDO	Hard	Yes	Narrow (<10 nm)	~100 μm
Saturated gain	Easy	Yes	Wide (>50 nm)	~500 μm

In this work, we utilize the broadband saturated gain of a semiconductor optical amplifier (SOA) waveguide to construct a non-reciprocal propagation area, and then compensate the power change with an appropriate linear loss waveguide which is designed as a hybrid surface plasmon polariton (SPP) waveguide [27]. The designed isolator supports duplex operation mode in a 59 nm operating band, and the isolation rate is as high as -20 dB, while the whole size of the device is as small as 465 μm × 0.35 μm.

2. Non-Reciprocal Transmission in Saturated Gain Waveguide

There is an important property of non-reciprocal transmission in a saturated gain waveguide. When light only inputs to one port of the waveguide with different powers (simplex operation mode), the output powers are identical after propagating over a long enough distance. The model of saturated gain is described in [28–31] as

$$G = \frac{G_0}{1 + P/P_s} - \alpha \tag{1}$$

where P is the power of light propagating in the saturated gain waveguide, P_s is the saturated parameter, G_0 is the gain coefficient for small signals, and α is the linear loss of the waveguide. Figure 1 shows the relationship between G and P. The zero point of the G–P curve is defined as cut-off power P_c, which can be expressed as

$$P_c = (\frac{G_0}{\alpha} - 1)P_s \tag{2}$$

When the power of the input light P is higher (lower) than P_c, the gain coefficient G is smaller (greater) than zero, and then P is going to decrease (increase) to P_c. It can be found that the gain coefficient G convergences to zero as shown in Figure 2a,b after a long enough propagating distance, and the output power P convergences to P_c which corresponds to the zero-gain coefficient.

When light signals are input into both of the two ports of a waveguide (duplex operation mode), Equation (1) is changed as

$$G(L) = \frac{G_0}{1 + [P_1(L) + P_2(L)]/P_s} - \alpha \tag{3}$$

where P_1 and P_2 are the power of light signals input from the right and left ports, respectively. In addition, P_1 and P_2 satisfy the following relations and conditions:

$$\tfrac{dP_1}{dL} = GP_1, \quad \tfrac{dP_2}{dL} = -GP_2 \tag{4}$$

$$\frac{dP_1}{dL}|_{L\to\infty} = 0, \quad \frac{dP_2}{dL}|_{L\to\infty} = 0 \tag{5}$$

Assuming that L_w is long enough to meet the boundary conditions, the solutions can be obtained by combining Equations (3)–(5) as

$$P_1(L_w) + P_2(L_w) = P_c, \quad P_2(0) + P_1(0) = P_c \tag{6}$$

Evidently, the sum of the input power at the right port and the output power at the left port is equal to the sum of the output power at the right port and the input power at the left port, and the value is exactly equal to P_c.

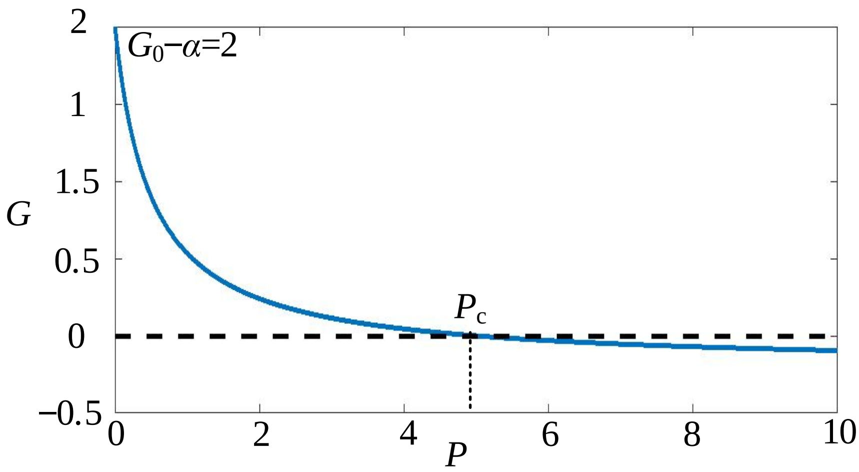

Figure 1. Blue line: Relation between the gain coefficient G and light power P. P_c is the cut-off power. Parameters of this case. The result is simulated with G_0 = 2.2, P_s = 0.5, and α = 0.2. Dotted: G = 0.

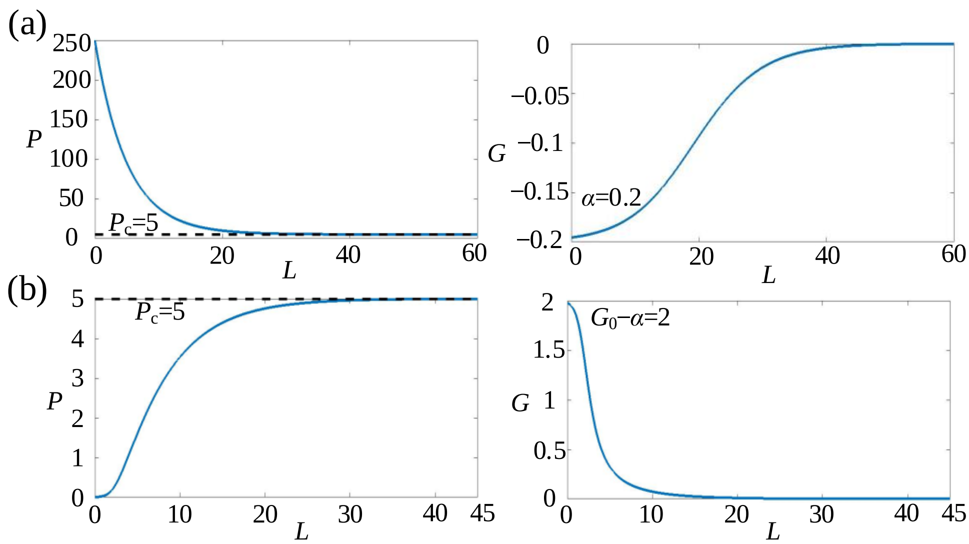

Figure 2. Blue line: Theoretical curves of functions $P(L)$ and $G(L)$ when the input power is (**a**) lower and (**b**) higher than P_c. Dotted: P_c = 5.

3. Isolator Model

Using the saturated gain model, we propose a sketchy model, supporting both the simplex and duplex operation modes, and then investigate the relationship between device size and performance. Exploiting the preceding demonstrations of Equations (1)–(6), the property of a saturated gain waveguide can be summed up as the illustration in Figure 3a. P_{o1} is the output power of P_H, and P_{o2} is the output power of P_L, where $P_H >> P_L$, and P_{o1}

$\approx P_{o2} \approx P_H \approx P_c$. Connecting a linear loss element to the saturated gain waveguide, the isolator model is obtained as shown in Figure 3b.

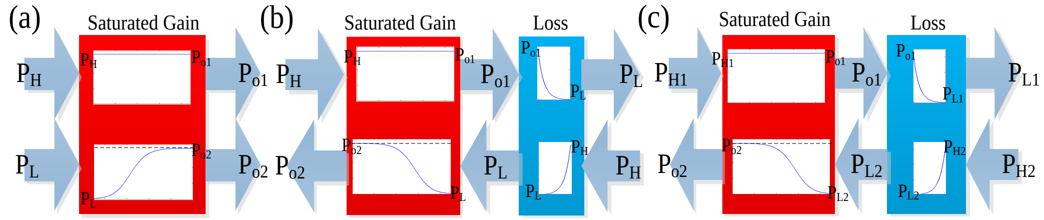

Figure 3. (**a**) Saturated gain property, (**b**) schematic diagram of simplex operating mode and (**c**) duplex operating mode. $P_H >> P_L$, $P_{o1} \approx P_{o2} \approx P_H \approx P_c$.

In the simplex operating mode, only one of the two ports of the device allows for the input of light signals. As shown in Figure 3b, when the light transmits from the left side to the right side, and its power is as high as $P_H \approx P_c$, the power can only be gained a little and becomes P_{o1} because of the saturated gain property; then, it decays to $P_L << P_H$ after transmitting through the additional loss element. By contrast, if light with power P_H is input from the right side, its power will decay to P_L first, and then grow to P_{o2} which is very close to P_H.

In the duplex operating mode, both of the two ports are inputs as shown in Figure 3c, it can be understood that $P_{H1} + P_{o2} = P_{L2} + P_{o1} = P_c$ in terms of Equation (6). If $P_{H1} = P_c$, it is clear that $P_{o2} = P_c/2 >> P_{L1}$. The isolation for backward signals is kept when the forward signals are transmitted through it. It should be noted that the operating power of duplex mode is half that of simplex in the same device.

The above discussion is based on the theory demonstrated in Equations (4) and (5), a theory that demands enough waveguide length. Here, a more detailed analysis is given to demonstrate how long that required length is. The design isolation ratio of the isolator r is defined as

$$r = \frac{T_L}{T_R} \tag{7}$$

where T_L is the transmission of input from the left and T_R is the transmission of input from the right. Firstly, we discuss the simplex operation mode. The P–L curve of a saturated gain waveguide for small signal input is plotted in Figure 4a in accordance with the numerical solution of

$$\frac{P + P_s}{P} dP = (P_s G_0 - \alpha P_s - \alpha P) dL \tag{8}$$

and the "enough amount of length" of the saturated gain waveguide can be found in Figure 4a as L_{t1}, which considers the output power tolerance as $t \times P_c$. Connecting a linear loss waveguide which decays the input power from P_c to $r_s P_c$ (r_s is the isolation ratio of simplex operation mode), the asymmetric transmission phenomenon can be observed in Figure 4b,c.

Next, we discuss the duplex operation mode. Similar to the simplex operation mode, the P–L curve of the saturated gain waveguide is also needed to find the "enough amount of length" L_{t2} as shown in Figure 5a. Further, connecting a linear loss waveguide which decays the input power from P_c to $r_d P_c/2$ (r_d is the isolation ratio of duplex), the P–L curve becomes Figure 5b for different propagating directions, and the asymmetric transmission can be observed. It should be noted that the main difference between simplex and duplex is the operation power. The operation power of duplex is half of that in simplex. Comparing simplex operation mode with duplex operation mode in the same system, it can be found that their operation powers are different. The operation power of duplex changed to $P_c/2$, which is half that of the simplex operation mode.

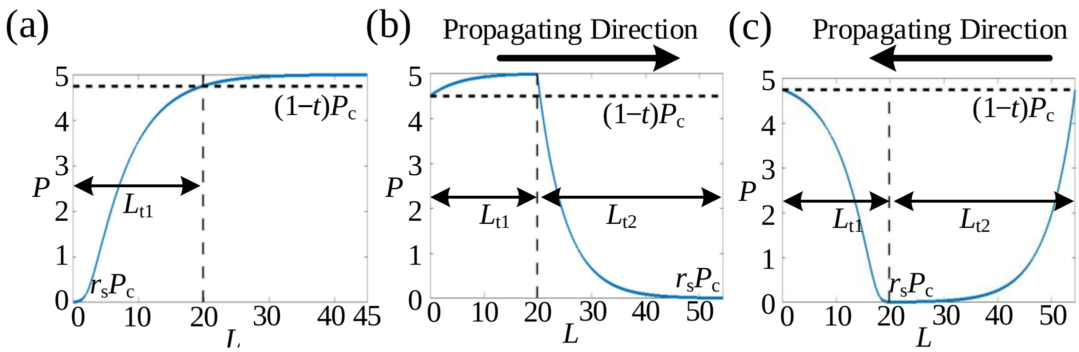

Figure 4. Blue line: Simulated results of propagation properties of the saturated gain waveguide (**a**), the proposed isolator when signals transmit forward (**b**) and backward (**c**).

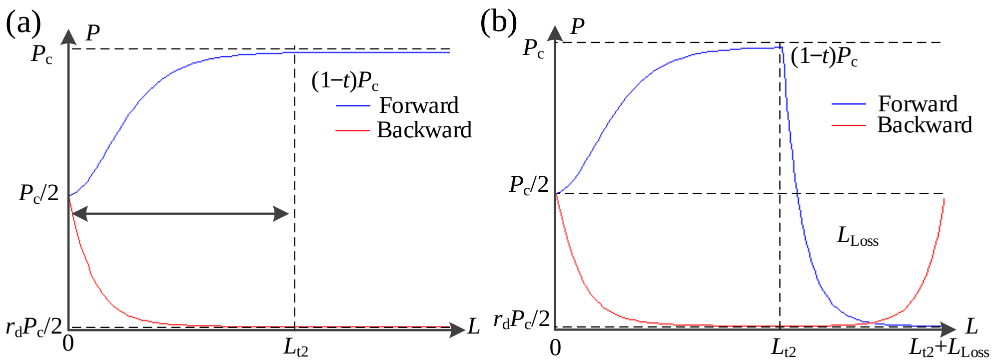

Figure 5. Simulated results of propagation properties of (**a**) the saturated gain waveguide and (**b**) connecting a linear loss waveguide in the isolator working at duplex mode.

4. Device Designing

Then, we give a practical design of an on-chip optical isolator in accordance with the model described in Figure 3. The design is made up of an SOA waveguide covered by metal, which provides saturated gain with a linear loss α fitting the mathematical model in Equation (1). Figure 6a exhibits the schematic of our design. The isolator consists of two parts, the gain part and the loss part. The cross-sections of the two parts are the same, shown in Figure 6b, while the lengths and pump currents are different. For the gain part, the length is L_{SOA} = 450 µm, and the pump current is 90 mA, corresponding to the parameters P_s = 3.41 mW and G_0 = 0.3 µm^{-1} at 1.55 µm operation wavelength [19–22]. For the loss part, the length is only L_D = 15 µm, and no pump is utilized in it. Figure 6b shows the layer structure of the cross-section of the proposed design. It can be seen that the SOA waveguide is an SPP waveguide consisting of a metal layer (exploited as an electrode), a p-type InP layer, an n-type InP layer and an InGaAsP quantum well layer [18]. It should be noted that the parameters P_s and G_0 are of the material, not of the SPP mode employed as shown in Figure 6c. The effective index of the SPP mode is 3.03 + i0.0176, and the decayed coefficient α is 0.1426 µm^{-1} in terms of the imaginary effective index 0.0197. Meanwhile, the P_s and G_0 become 3.5365 mW and 0.1687 µm^{-1}, respectively, and the cut-off power P_c is 643 µW. Accordingly, it can be calculated using Equation (8) and the FDTD method or the Runge–Kutta method that 15 µm L_D provides a bidirectional 20 dB decay to make the 643 µW input power decay to 6.43 µW; additionally, the 450 µm L_{SOA} ensures the 6.43 µW low-power signal increases back to 643 µW, and the 643 µW signal maintains its power, which realizes non-reciprocal transmission.

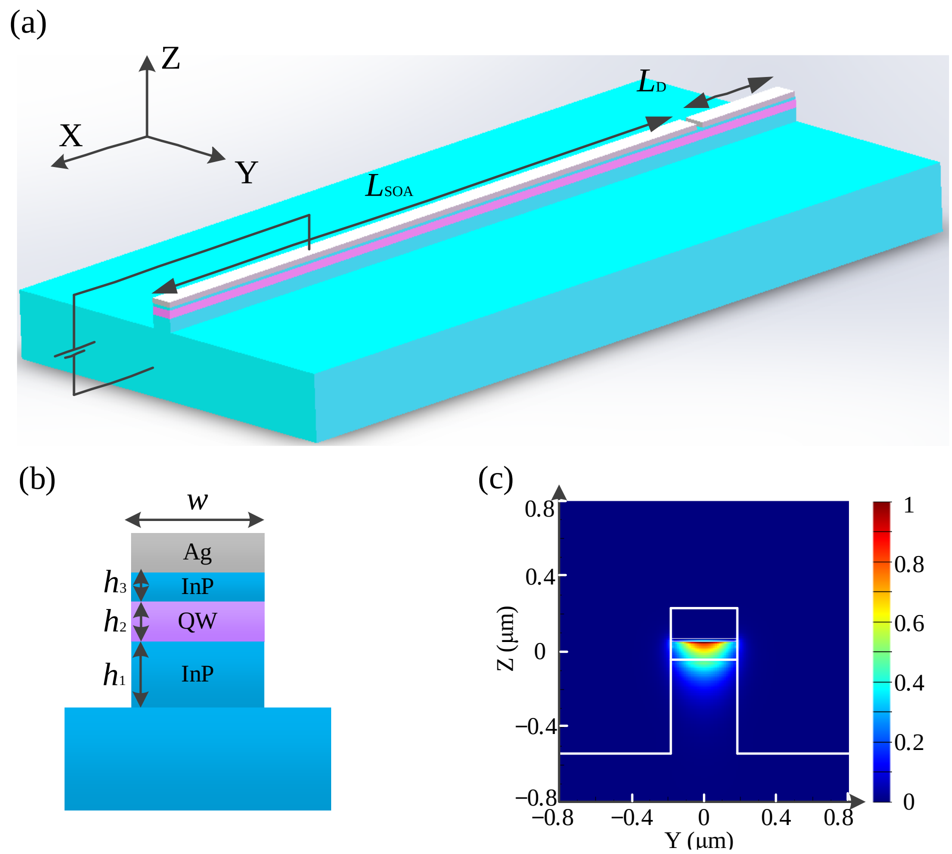

Figure 6. (**a**) Schematic of the isolator, L_{SOA} = 450 µm, L_D = 15 µm. (**b**) Layer structure of SOA waveguide, h_1 = 0.5 µm, h_2 = 0.2 µm, h_3 = 0.01 µm, w = 0.35 µm. (**c**) Normalized electrical field distribution of fundamental TM mode. The length of SOA L_{SOA} and loss part L_D are designed to support an on-chip optical isolator with a 643 µW input power and 20 dB isolation rate. L_D = 15 µm provides a bidirectional 20 dB decay to make 643 µW input power decay to 6.43 µW. L_{SOA} = 450 µm ensures the 6.43 µW low-power signal increases back to 643 µW, and the 643 µW signal maintains its power.

According to Equation (8) and the parameters (α, P_s and G_0), the solid blue line in Figure 7a can be calculated numerically. It is clear that a 6.43 µW signal increases to 642.5 µW (99.92% of P_c) after propagating a 450 µm distance. The finite-difference time-domain (FDTD) [32,33] result (the red dashed line) also fits the analytical solution (calculated using Equations (4) and (5) with original code) as shown in Figure 7a. Meanwhile, if a signal with a power of 643 µW is input, the P–L curve changes to Figure 7b. Connecting a 15 µm loss waveguide with the SOA mentioned above, the function of an isolator can be realized; the P–L curves (signal inputs from the left and right), similar to Figure 4b,c, are given in Figure 8a,b, respectively.

Our design also supports broadband operation. Exploiting the broadband gain spectrum of the SOA, we have calculated the broadband transmission characteristics of the SOA when the input power is 643 µW and 6.43 µW in Figure 9a. Combining with the transmission spectrum of the loss part, Figure 9 can be obtained to illustrate the output power spectrum of both directions of the isolator and the spectrum of the isolating factor, F, expressed by P_{out}/P_{in}. Further, considering F > 99 as a criterion, the bandwidth of the isolator is calculated to be as broad as 59 nm. All the results are simulated.

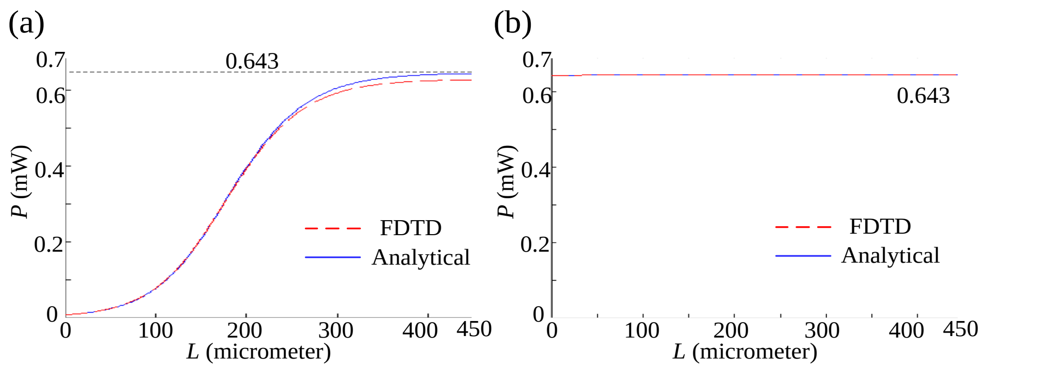

Figure 7. FDTD-simulated and analytical results of relation between P and L when a signal with (**a**) 6.43 µW and (**b**) 643 µW inputs power. Black dotted lines: P = 0.643.

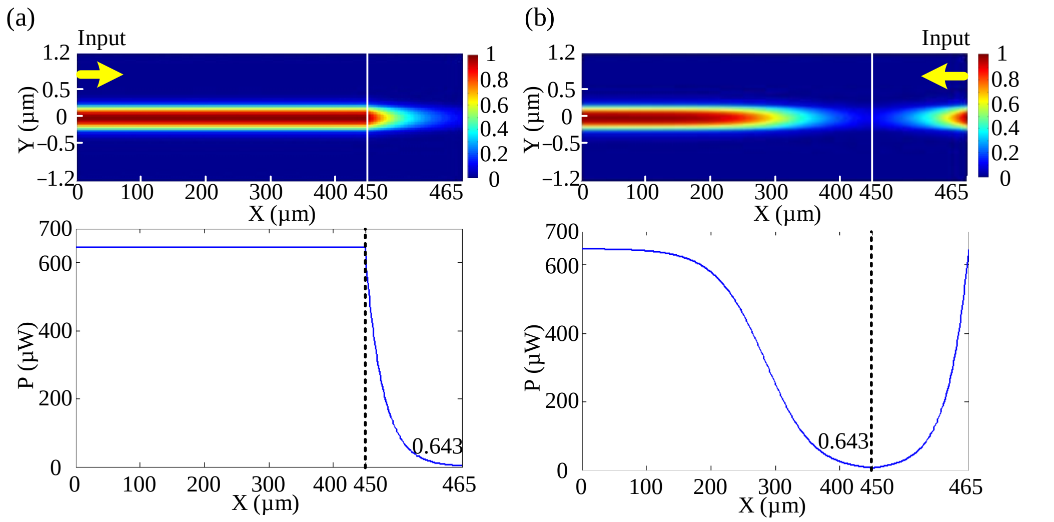

Figure 8. Blue lines: Conditions when light is input (**a**) from right to left and (**b**) from left to right. Dotted lines: X = 450.

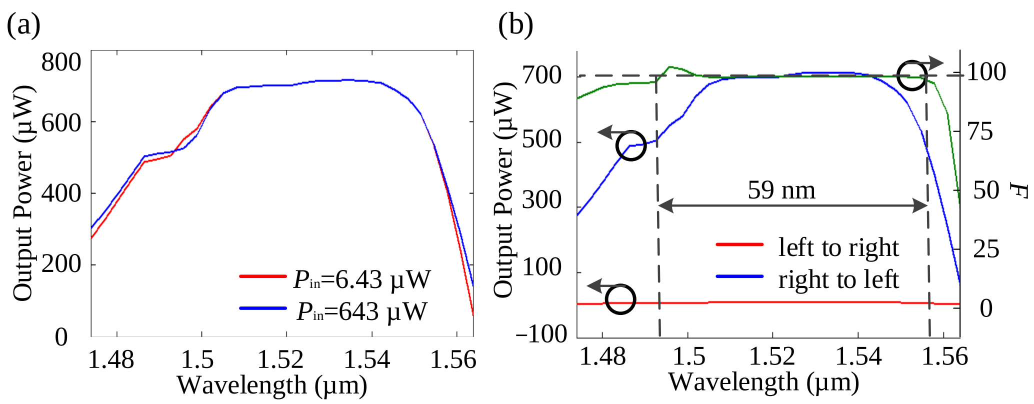

Figure 9. (**a**) Simulated broadband transmission characteristic of the SOA. (**b**) Simulated broadband transmission and isolating factor of the whole device.

It has already been pointed out in Figure 5 that duplex operation mode exhibits lower operation power compared to simplex, so it is important to find an effective way to adjust operation power. The pump current is the key to controlling operation power. The operation power varies with the pump current of the gain part. Figure 10a gives the relation between P and L of the SOA with different pump currents at 1.55 µm, and the corresponding operation power can be calculated in Figure 10b. If we change the operation mode from simplex to duplex, and hope to maintain operation power, we can increase pump currents to fit it.

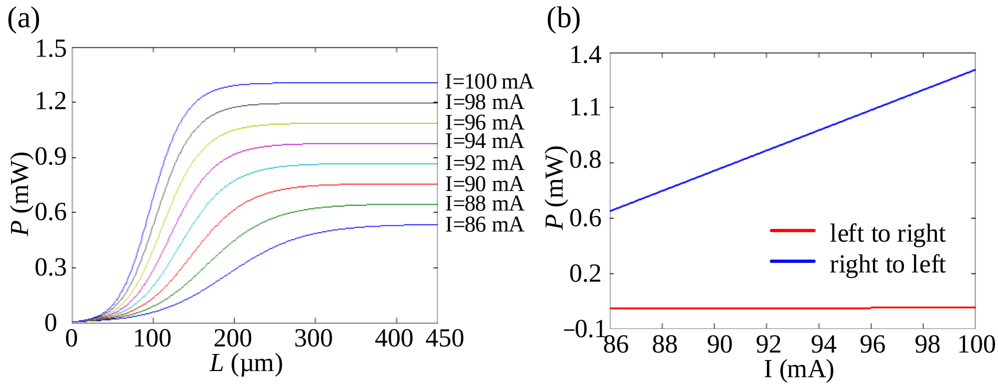

Figure 10. (**a**) *P*–*L* curves of the SOA with different pump currents. (**b**) Operation power of the isolator with different pump currents. All the curves are simulated using FDTD.

5. Conclusions

In summary, we have proposed a novel method of designing the broadband optical isolator based on nonlinear gain, and the fundamental theory of the isolator is completely demonstrated. With the guidance of this theory, we have designed a broadband optical isolator working at a wide wavelength scope, from 1.500 μm to 1.559 μm. In addition, the isolator works at different powers with the same isolated factor, 100, when the current pump is changed. Moreover, the length of the whole device is only 465 μm, and the footprint area is as small as 465 μm × 0.35 μm. The size of the device satisfies the requirement of the application of photonic integrated circuits, and in particular, it can be applied to eliminate integrated backscatter, protect the source and construct complex communication topology in photonic integration.

Author Contributions: Conceptualization, M.X.; methodology, H.T.; software, H.D. and M.W.; validation, H.T. and H.D.; writing—original draft preparation, M.X.; writing—review and editing, M.X.; project administration, M.X.; funding acquisition, M.X. All authors have read and agreed to the published version of the manuscript.

Funding: This research was funded by the Natural Science Basic Research Program of Shaanxi, grant number 2022JQ-634; the Scientific Research Plan of Shaanxi Education Department, grant number 22JK0301 and the Natural Science Basic Research Program of Shaanxi, grant number 2022JQ-175.

Institutional Review Board Statement: Not applicable.

Informed Consent Statement: Not applicable.

Data Availability Statement: The data are contained within the article.

Conflicts of Interest: The authors declare no conflicts of interest.

References

1. Ma, H.; He, Z.; Hotate, K. Reduction of backscattering induced noise by carrier suppression in waveguide-type optical ring resonator. *J. Light. Technol.* **2011**, *29*, 85–90. [CrossRef]
2. Zhang, Z.; Zhu, L. Nonreciprocal thermal photonics for energy conversion and radiative heat transfer. *Phys. Rev. Appl.* **2022**, *18*, 027001. [CrossRef]
3. Shui, T.; Yang, W.X.; Cheng, M.T.; Lee, R.K. Optical nonreciprocity and nonreciprocal photonic devices with directional four-wave mixing effect. *Opt. Express* **2022**, *30*, 6284–6299. [CrossRef] [PubMed]
4. Ehlers, P.; Silander, I.; Wang, J.; Foltynowicz, A.; Axner, O. Fiber-laser-based noise-immune cavity-enhanced optical heterodyne molecular spectrometry incorporating an optical circulator. *Opt. Lett.* **2014**, *39*, 279–282. [CrossRef]
5. Wang, X.; Hao, R.; Fan, P.; Hu, L.; Ye, B.; Zou, Y.; Jin, S. Effective enhancement of the non-Hermitian corner skin effect in reciprocal photonic crystals. *Opt. Lett.* **2024**, *49*, 554–557. [CrossRef] [PubMed]

6. He, H.; Zhang, S.; Qi, J.; Bo, F.; Li, H. Faraday rotation in nonreciprocal photonic time-crystals. *Appl. Phys. Lett.* **2023**, *122*, 051703. [CrossRef]
7. Mimbs, J.W.; O'Donnell, M.; Miller, J.G.; Sobel, B.E. Detection of cardiomyopathic changes induced by doxorubicin based on quantitative analysis of ultrasonic backscatter. *Am. J. Cardiol.* **1981**, *47*, 1056–1060. [CrossRef]
8. Dong, C.; Shen, Z.; Zou, C.; Zhang, Y.; Fu, W.; Guo, G. Non-reciprocal light storage in a silica microsphere. In Proceedings of the 2015 Conference on Lasers and Electro-Optics (CLEO), San Jose, CA, USA, 10–15 May 2015; pp. 1–2.
9. Zheng, Y.; Yang, J.; Shen, Z.; Cao, J.; Chen, X.; Liang, X.; Wan, W. Optically induced transparency in a micro-cavity. *Light Sci. Appl.* **2016**, *5*, e16072. [CrossRef]
10. Chang, L.; Jiang, X.; Hua, S.; Yang, C.; Wen, J.; Jiang, L.; Li, G.; Wang, G.; Xiao, M. Parity–time symmetry and variable optical isolation in active-passive-coupled microresonators. *Nat. Photonics* **2014**, *8*, 524–529. [CrossRef]
11. Ahmed, W.; Farhat, M.; Staliunas, K.; Zhang, X.; Wu, Y. Machine learning for knowledge acquisition and accelerated inverse-design for non-Hermitian systems. *Commun. Phys.* **2023**, *6*, 2. [CrossRef]
12. Peng, B.; Özdemir, Ş.; Lei, F.; Monifi, F.; Gianfreda, M.; Long, G.; Fan, S.; Nori, F.; Bender, C.; Yang, L. Parity–time-symmetric whispering-gallery microcavities. *Nat. Phys.* **2014**, *10*, 394–398. [CrossRef]
13. Shen, Z.; Dong, C.; Chen, Y.; Xiao, Y.; Sun, F.; Guo, G. Compensation of the Kerr effect for transient optomechanically induced transparency in a silica microsphere. *Opt. Lett.* **2016**, *41*, 1249–1252. [CrossRef] [PubMed]
14. Bi, L.; Hu, J.; Jiang, P.; Kim, D.; Dionne, G.; Kimerling, L.; Ross, C. On-chip optical isolation in monolithically integrated non-reciprocal optical resonators. *Nat. Photonics* **2011**, *5*, 758–762. [CrossRef]
15. Tian, H.; Liu, J.; Siddharth, A.; Wang, R.; Blésin, T.; He, J.; Kippenberg, T.; Bhave, S. Magnetic-free silicon nitride integrated optical isolator. *Nat. Photonics* **2021**, *15*, 828–836. [CrossRef]
16. Kittlaus, E.; Jones, W.; Rakich, P.; Otterstrom, N.; Muller, R.; Rais-Zadeh, M. Electrically driven acousto-optics and broadband non-reciprocity in silicon photonics. *Nat. Photonics* **2021**, *15*, 43–52. [CrossRef]
17. Wang, C.; Fu, Z.; Mao, W.; Qie, J.; Stone, A.; Yang, L. Non-Hermitian optics and photonics: From classical to quantum. *Adv. Opt. Photonics* **2023**, *15*, 442–523. [CrossRef]
18. Fujita, J.; Levy, M.; Osgood Jr, R.; Wilkens, L.; Dötsch, H. Waveguide optical isolator based on Mach–Zehnder interferometer. *Appl. Phys. Lett.* **2000**, *76*, 2158–2160. [CrossRef]
19. Vanwolleghem, M.; Gogol, P.; Beauvillain, P.; Van Parys, W.; Baets, R. Design and optimization of a monolithically integratable InP-based optical waveguide isolator. *JOSA B* **2007**, *24*, 94–105. [CrossRef]
20. Van Parys, W.; Moeyersoon, B.; Van Thourhout, D.; Baets, R.; Vanwolleghem, M.; Dagens, B.; Decobert, J.; Le Gouezigou, O.; Make, D.; Lagae, L. Transverse magnetic mode non reciprocal propagation in an amplifying AlGaInAs/InP optical waveguide isolator. *Appl. Phys. Lett.* **2006**, *88*, 071115. [CrossRef]
21. Qin, J.; Deng, L.; Xie, J.; Tang, T.; Bi, L. Highly sensitive sensors based on magneto-optical surface plasmon resonance in Ag/CeYIG heterostructures. *AIP Adv.* **2015**, *5*, 017118. [CrossRef]
22. Shui, K.; Nie, L.; Zhang, Y.; Peng, B.; Xie, J.; Deng, L.; Bi, L. Design of a compact waveguide optical isolator based on multimode interferometers using magneto-optical oxide thin films grown on silicon-on-insulator substrates. *Opt. Express* **2016**, *24*, 12856–12867. [CrossRef] [PubMed]
23. Yu, Z.; Fan, S. Complete optical isolation created by indirect interband photonic transitions. *Nat. Photonics* **2009**, *3*, 91–94. [CrossRef]
24. Shen, Z.; Zhang, Y.; Chen, Y.; Zou, C.; Xiao, Y.; Zou, X.; Sun, F.; Guo, G.; Dong, C. Experimental realization of optomechanically induced non-reciprocity. *Nat. Photonics* **2016**, *10*, 657–661. [CrossRef]
25. Galiffi, E.; Tirole, R.; Yin, S.; Li, H.; Vezzoli, S.; Huidobro, P.; Silveirinha, M.; Sapienza, R.; Alù, A.; Pendry, J. Photonics of time-varying media. *Adv. Photonics* **2022**, *4*, 014002. [CrossRef]
26. Shi, Y.; Yu, Z.; Fan, S. Limitations of nonlinear optical isolators due to dynamic reciprocity. *Nat. Photonics* **2015**, *9*, 388–392. [CrossRef]
27. Palik, E.D. *Handbook of Optical Constants of Solids*; Academic Press: New York, NY, USA, 1998.
28. Dutta, N.K.; Wang, Q. *Semiconductor Optical Amplifiers*; World Scientific Press: Singapore, 2013.
29. Sugawara, M.; Mukai, K.; Nakata, Y.; Ishikawa, H.; Sakamoto, A. Effect of homogeneous broadening of optical gain on lasing spectra in self-assembled InxGa1-xAs/GaAs quantum dot lasers. *Phys. Rev. B* **2000**, *61*, 7595. [CrossRef]
30. Durhuus, T.; Mikkelsen, B.; Stubkjaer, K. Detailed Dynamic Model for Semiconductor Optical Amplifiers and Their Crosstalk and Intermodulation Distortion. *J. Light. Technol.* **1992**, *10*, 1056–1065. [CrossRef]
31. Connelly, M.J. *Semiconductor Optical Amplifiers*; Springer Science & Business Media: Berlin/Heidelberg, Germany, 2007.
32. Sullivan, D.M. *Electromagnetic Simulation Using the FDTD Method*; John Wiley & Sons: Hoboken, NJ, USA, 2013.
33. Available online: www.photond.com (accessed on 1 October 2020).